N_2 Chemisorption on Stepped Pt Surfaces. Control by 2-D and 1-D Precursor Behavior†

C. Emil Tripa, Tykhon S. Zubkov, and John T. Yates, Jr.*

Surface Science Center, Department of Chemistry, University of Pittsburgh, Pittsburgh, Pennsylvania 15260

Received: August 29, 2000

Nitrogen adsorption uptake at 88 K and temperature-programmed desorption (TPD) experiments were done on two stepped platinum surfaces, Pt(335) and Pt(779). N_2 adsorption occurs only on the step sites, and the saturation coverages measured on these surfaces were $(1.51 \pm 0.09) \times 10^{14}$ and $(1.01 \pm 0.16) \times 10^{14}$ cm^{-2}, respectively, indicating a higher fractional population of widely separated step sites compared to closely spaced step sites. The adsorption kinetics revealed that the adsorption is mediated by terrace and step precursors. The N_2 initial sticking probability is 0.91 ± 0.06 (average of six measurements) on the Pt(335) surface and 0.68 ± 0.07 (average of five measurements) on the Pt(779) surface. The binding energy of N_2 at step sites, determined from experimental and simulated TPD curves, is -0.50 eV at zero coverage and decreases monotonically to -0.44 eV at saturation coverage on both surfaces. The equilibrium thermodynamics of N_2 adsorbed on either of the two stepped Pt surfaces are the same. The role of terrace width on the initial sticking probability is discussed for adsorption on stepped surfaces.

I. Introduction

Molecular nitrogen chemisorption on Pt surfaces exhibits quite interesting behavior. It only chemisorbs irreversibly at temperatures below 180 K,[1,2] and then only on defect sites.[1−3] The defect sites responsible for N_2 chemisorption are Pt atoms with low coordination numbers: the edges of the step sites[1,3] and perhaps the kink sites. No chemisorption has been detected on Pt(111) terrace sites above 60 K. On step sites, N_2 chemisorbs in an atop configuration only, with a N−N stretching mode at $\sim$2231 cm^{-1} at saturation coverage.[1] Below 60 K, an IR-inactive physisorbed N_2 phase has been reported on a Pt(111) surface which, at 27 K, is in equilibrium with 0.07 monolayer of IR-active weakly chemisorbed N_2 with a stretching mode frequency of 2266 cm^{-1}.[4] Molecular nitrogen is thus a chemical sensor for defect sites on Pt monocrystal and Pt catalyst surfaces[1,3] when the adsorption temperature is above the desorption temperature of the species with the 2266 cm^{-1} mode. The N_2 binding energy on step sites must be small since many other molecules displace it from the adsorbed phase.[1,5,6] A density functional theory calculation, within the generalized gradient approximation, predicted a binding energy of -0.34 eV at 50% coverage on Pt(112) step sites.[1] In the present study, we show that the adsorption energy decreases from -0.50 eV at zero coverage to -0.44 eV at 50% step-site coverage on Pt(335) and Pt(779).

At saturation coverage, N_2 molecules are located only at step sites and form 1-D chains.[1] The adsorption and desorption experiments presented here show that, at saturation, there is about one molecule present on every other step Pt atom and the spacing is controlled by lateral repulsive interactions. More interestingly, both the adsorption and the desorption are mediated by mobile precursor species adsorbed on *both* types of surface sites. The average area sampled by the terrace-site precursor, relative to the average terrace width, controls the magnitude of the initial sticking probability, in addition to the efficiency of the energy transfer from precursor to the substrate. Thus, a stepped Pt surface with wide terraces will exhibit a lower sticking probability for N_2 chemisorption because of the higher probability of N_2 desorption from the precursor prior to trapping at a step site. The step-bound precursors experience a larger trapping force due to an increased surface interaction in the trough, and their motion is confined along the steps. The adsorption precursors, wandering in a 2-D space on the terraces and a 1-D space on the steps, convene together using the surface as template and form a 1-D phase localized on the periodic step sites.

At a higher partial pressure of nitrogen, the N_2 saturation coverage on both stepped surfaces can be increased due to the availability of empty step sites. However, when the external N_2 pressure is restored to UHV conditions ($\sim 1.0 \times 10^{-10}$ Torr), the excess of nitrogen adsorbed on the surface desorbs immediately to reestablish the new equilibrium conditions. These experiments are fully presented in another study published in this issue (following paper).[7] These experiments revealed that the adsorption of excess nitrogen follows a Langmuir isotherm, although the mechanism of adsorption involves precursors and excludes direct adsorption from the gas phase.

In this study, we use two stepped Pt surfaces, Pt(335) and Pt(779), and compare them to each other in adsorption and desorption experiments. The Pt(335) surface consists of one-atom-high step sites of (001) orientation and four-atom-wide terrace sites of (111) orientation. The Pt(779) surface contains the same types of sites with a terrace width which is twice as wide, or in other words, it has half the density of step sites as the Pt(335) surface. We find that all the thermodynamic properties of N_2 on the two surfaces are essentially the same, except for the initial sticking probability and the strength of the lateral interaction between step-bound N_2 molecules across the terrace. These properties depend strongly on the terrace width.

II. Experiment

All experiments were done in an ultrahigh vacuum (UHV) chamber with a base pressure lower than 1.0×10^{-10} Torr. The

† Part of the special issue "John T. Yates, Jr. Festschrift".

10.1021/jp0031193 CCC: $20.00
Published on Web 02/22/2001

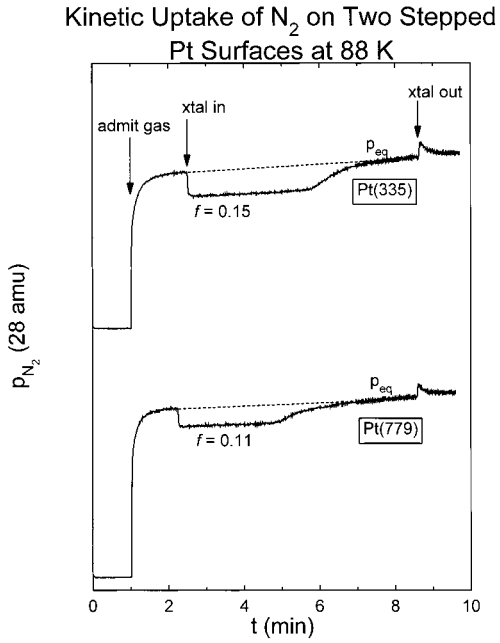

Figure 1. N_2 adsorption uptake curves at 88 K on Pt(335) and Pt(779) surfaces. Gaseous N_2 is admitted into the UHV system through a molecular beam effusion doser at the moment "admit gas", and the partial pressure of N_2 is monitored with a mass spectrometer. When N_2 reaches a nearly steady pressure, the crystal is translated into the beam ("xtal in") and its front surface starts to adsorb. The N_2 partial pressure drops at this point, and in time, after the crystal front surface becomes saturated, it returns to the steady pressure value (p_{eq}). The moment when the crystal is translated out of the gas beam ("xtal out") is accompanied by a desorption feature to be discussed in the following paper in this issue.[7] The factor *f* represents the fraction of the gas effused through the doser which is adsorbed on the surface, as measured from the relative pressure drop at the initial stage of adsorption.

system was equipped with an unshielded quadrupole mass spectrometer (QMS), used in the present work to accurately measure partial pressure changes during adsorption and desorption.

Two stepped Pt surfaces, (335) and (779), were used in this work. The surfaces were prepared as two opposed faces on the same Pt(111) monocrystal. The preparation and characterization of these stepped Pt surfaces have been described in detail elsewhere.[1] The crystal was spot-welded to two 1.0 mm W wires for efficient heating and cooling. With this mounting, a base temperature of 88 K was reproducibly achieved using liquid N_2 as coolant. Linearized temperature ramps of the substrate in the TPD experiments were done with a digital temperature programmer described previously.[8]

$^{14}N_2$(g) (99.9999% purity; natural isotopic abundance) was dosed onto the crystal surface through an absolutely calibrated and collimated capillary array doser with a 22 mm diameter active area.[9] The flow rate is controlled by an internal pinhole. The capillary array doser creates an effused and quasi-collimated molecular beam with known throughput and cross-sectional distribution of the flux.[10] Gas dosing from a beam minimizes the partial pressure rise of the gas being dosed and the exposure of the back surface of the crystal to the gas of interest during the adsorption measurements. For our crystal geometry, the flux delivered was 1.7×10^{12} N_2 $Torr^{-1}$ s^{-1} cm^{-2}, corresponding to a crystal interception efficiency, $\alpha = 0.16$.[10]

The adsorption experiment, illustrated in Figure 1, is a version of the King and Wells method, developed in 1972.[11] A beam of N_2 effusing out of a multicapillary doser is incident on our 15 mm diameter Pt single crystal, located at a known distance from the doser. The QMS in our UHV system, positioned away from the direct line of sight of the doser and crystal, measures the N_2 pressure change (i.e., the random flux). When the gas is admitted, the pressure rises quickly and attains a nearly steady value which corresponds to a quasi-equilibrium situation where the number of molecules transported into the UHV system is balanced by the number pumped out. The crystal is then translated into the N_2 beam, and a fraction of the N_2 is adsorbed, causing the random flux of N_2 to decrease. This part of the uptake curve contains the most important information and is used to compute the sticking coefficient and the absolute coverage. Once the crystal surface directly exposed to the N_2 beam has saturated, the random-flux pressure asymptotically approaches the dashed line in Figure 1. The uptake is complete when the QMS signal merges completely with the dashed line—the moment when all the molecules incident to the crystal surface are reflected off into the gas phase.

III. Results

A. Adsorption Measurements. A typical N_2 adsorption uptake measurement is shown in Figure 1. The meaning of the various parts of the uptake curve has been described above. The curve in the adsorption stage (between "xtal in" and "xtal out") is parallel to the dashed line (the random-flux behavior of N_2 in the absence of direct adsorption onto the surface) over a large period of time, indicating a constant sticking coefficient. Only in the late stages of adsorption does the sticking coefficient drop gradually to zero. The saturation coverage on the two surfaces is directly proportional to the area contained between the uptake curve and the dashed line, and is larger for the Pt(335) surface than for the Pt(779) surface. The factor *f*, defined as the ratio of the pressure drop at the time "xtal in" to the total pressure rise before this moment, represents the fraction of the N_2 beam adsorbed on the substrate. The value of the *f* factor cannot exceed the fraction of the N_2 beam impinging on the substrate (called the interception efficiency, α, above), 0.16 in our case. The initial sticking coefficient of N_2 adsorption is close to 0.94 on the Pt(335) surface and close to 0.69 on the Pt(779) surface. The desorption feature accompanying the crystal translation out of the beam ("xtal out") is a real surface effect. The origin of this feature will be discussed in detail in part II of our study published in this issue (following paper).[7]

The relative sticking coefficient (or sticking probability), $S(t)/S_o$, can be calculated from the uptake curve with the following equation, first proposed by Madey:[12]

$$\frac{S(t)}{S_o} = \frac{1}{f}\left(1 - \frac{p(t)}{p_{eq}}\right) \qquad (1)$$

where p is the pressure, t is the time, S_o is the initial sticking probability, and p_{eq} is the steady pressure in the absence of direct adsorption from the beam. If the angular distribution of the gas emitted by the doser is known and the interception efficiency α can be accurately determined, the method allows one to measure absolute sticking probabilities ($S_o = f/\alpha$) and absolute coverages.

Figure 2 shows the absolute sticking probability dependence on the exposure, $S(\epsilon)$, calculated from uptake curves for the two crystal surfaces. During the adsorption, p_{eq} shown on Figure 1 is not really constant because the pumping speed of the UHV chamber for N_2 drops slightly. To eliminate complications associated with a changing pumping speed, p_{eq} is replaced by the dashed background curve in Figure 1.[13] In Figure 2, the exposure $\epsilon(t)$ is calculated as

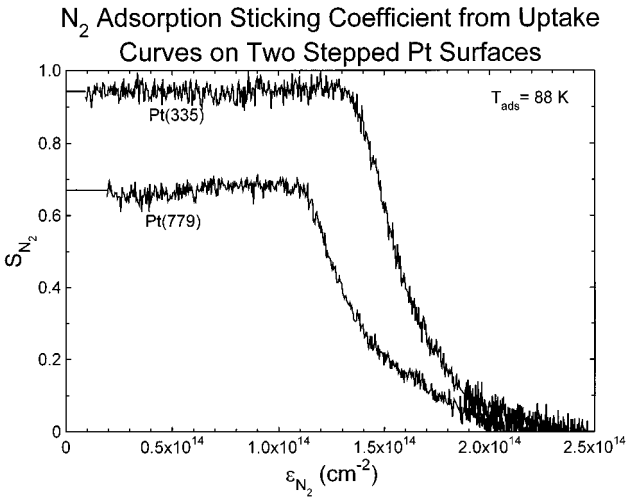

Figure 2. Absolute sticking coefficient of N_2 at 88 K as a function of exposure on the Pt(335) and Pt(779) stepped surfaces. These curves are derived from the adsorption parts of the curves shown in Figure 1 (see the text for derivation). The noise-free curves at initial exposures represent extrapolated values of the initial sticking coefficients, corresponding to adsorption prior to crystal translation into the N_2 molecular beam. In these regions, the preexposure was calculated from the random flux of N_2 impinging on the crystal as generated by the steady pressure in the UHV chamber.

$$\epsilon(t) = \frac{\alpha}{A_{\text{surf}}} Q(t - t_{\text{xtal in}}) + \epsilon_{\text{o}} \tag{2}$$

where A_{surf} is the area of the substrate surface exposed to the molecular beam and Q is the doser throughput. Prior to insertion into the beam, the substrate adsorbs an exposure, ϵ_{o}, from the random flux generated by admitting gas through the doser into the UHV system. We assumed that the crystal did adsorb N_2 within this time frame, and we computed the exposure as

$$\epsilon_{\text{o}}(t) = \frac{p(t)}{(2\pi mkT)^{1/2}}(t - t_{\text{admit gas}}) \tag{3}$$

to generate the initial smooth part of the curves shown in Figure 2. In this low-exposure region, we extrapolated the initial sticking coefficient measured in the uptake experiment to zero exposure. The initial coverage, corresponding to ϵ_{o}, is 6−13% of the final coverage in these experiments. For the two uptake curves selected to construct Figure 2, the initial sticking coefficients are 0.94 for the Pt(335) surface and 0.68 for the Pt(779) surface. For both surfaces, the saturation coverage is achieved with exposures near 2.5×10^{14} cm^{-2}, indicating that less than a quarter of the surface atoms act as adsorption sites for N_2.

The absolute coverage $\sigma(\epsilon)$ (cm^{-2}) is computed straightforwardly from curves such as those shown in Figure 2 according to the formula

$$\sigma(\epsilon) = \int_0^{\epsilon} S(\epsilon)\, \mathrm{d}\epsilon \tag{4}$$

which is based on the mathematical definition of the sticking probability, $S(\epsilon)$, as the derivative of the coverage with respect to exposure. We used 10 exposure points to build the coverage−exposure uptake curves shown in Figure 3 for the Pt(335) and Pt(779) surfaces. The ratio of the saturation coverages on the two stepped Pt surfaces as measured from the points at the highest exposure on each curve is 1.49 ± 0.25. The uptake curves in Figure 3 display an extended linear portion at lower

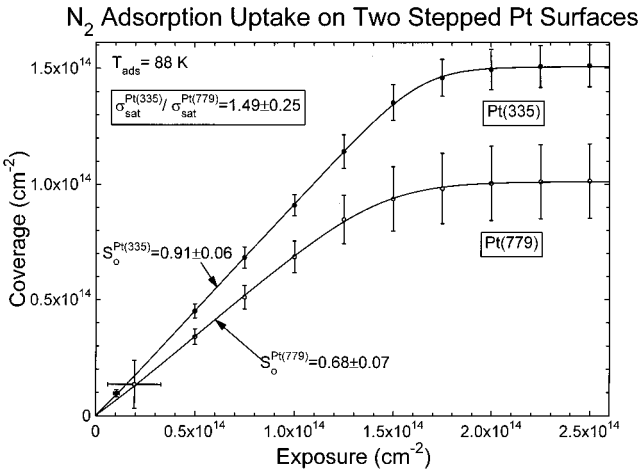

Figure 3. Coverage vs exposure curves for N_2 on Pt(335) and Pt(779) surfaces at 88 K and in equilibrium with less than 1.0×10^{-10} Torr of N_2 in the gas phase. The points are obtained by integration of the sticking coefficient as a function of exposure on curves such as those shown in Figure 2. Each vertical error bar represents a $\pm 2\sigma_{n-1}$ systematic deviation of a set of six adsorption uptake curves for the Pt(335) surface or five curves for the Pt(779) surface. In addition, the first point on each curve has a horizontal error bar to account for different initial exposures before each time the crystal is translated into the molecular beam. The ratio of the saturation coverages (σ_{sat}) on the two stepped Pt surfaces is calculated from the last point on each curve. S_{o} represents the initial sticking probability determined from straight-line fits of the initial part of each uptake curve. The solid lines are fits through the experimental points.

coverages, and overall, their shape therefore deviates significantly from Langmuirian adsorption kinetics. The initial sticking coefficients of N_2 adsorption are 0.91 ± 0.06 ($r^2 = 0.9999$) (average of six measurements) on the Pt(335) surface and 0.68 ± 0.07 ($r^2 = 0.9999$) (average of five measurements) on the Pt(779) surface (error bar $\pm 2\sigma_{n-1}$).

B. Nonisothermal Desorption Kinetics: Simulation and Experiment. We produced and analyzed a series of experimental and simulated N_2 TPD curves at different initial coverages to estimate the binding energy from the activation energy of desorption or the isosteric heat of adsorption. Figure 4 shows a family of experimental and simulated desorption spectra for each Pt surface under investigation. For both surfaces, the higher-temperature desorption state (158 K) develops first. This state broadens with increasing coverage, and its peak maximum shifts a total of ∼10 K to lower temperatures over the entire coverage range. Above a certain coverage, a lower-temperature desorption state becomes visible which develops to the saturation condition. Irrespective of the initial coverage, N_2 desorption is complete by 180 K, in agreement with previous reports on Pt(111) surfaces which contained artificially produced and natural defect sites.[2,6] The desorption feature at ∼90 K seen in the experiments is an artifact produced by the crystal holder.

In the simulation, the desorption was assumed to occur under quasi-equilibrium conditions. That is, the surface diffusion is so fast on the time scale of desorption that the adsorbate is maintained in equilibrium throughout the process, and the adsorbate can be characterized by its chemical potential, μ. At equilibrium, the chemical potential in the gas phase is equal to that in the adsorbate phase. The latter can be expressed in terms of the parameters of the potential energy surface (PES) and the lateral interaction between particles. This quasi-equilibrium approximation was developed by Payne and Kreuzer, and its treatment can be found elsewhere.[14,15] In this approximation,

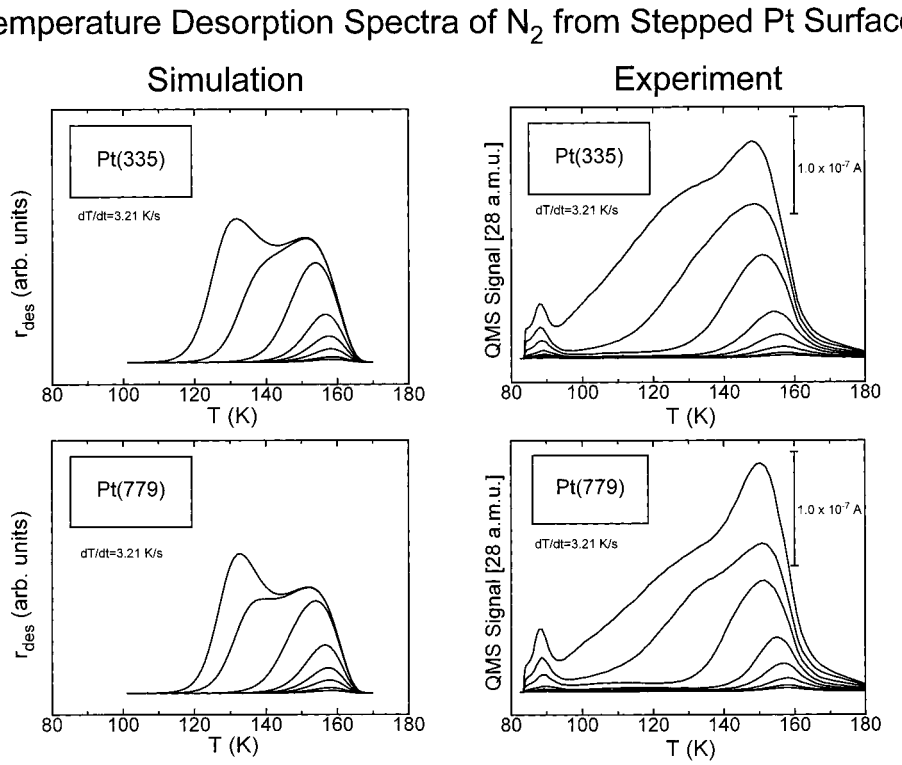

Figure 4. Simulated (left) and experimental (right) temperature-programmed desorption traces of N_2 at various initial coverages from Pt(335) (upper panels) and Pt(779) (lower panels) surfaces. The experimental curves are affected in the high-temperature desorption region by errors due to desorption from the backside of the crystal and from extraneous surfaces. The heating rate used in all the measurements and simulations was 3.21 K/s.

the rate of desorption, R_d, is expressed as

$$R_d = S(\theta)\frac{\theta}{(1-\theta)}a_S\frac{Z_{vib}Z_{rot}}{q_\nu q_\delta^{\,2} q_{hvib} q_{hrot}}\frac{kT}{h\lambda_{th}^{\,2}}\exp\left(\frac{V_o}{kT}+\frac{\mu_i}{kT}\right) \quad (5)$$

where $S(\theta)$ is the sticking coefficient, θ is the fractional coverage, a_S is the area of the unit cell, Z_{vib} and Z_{rot} are partition functions of the free molecule, q_{hvib} and q_{hrot} are partition functions of the molecule sitting in a PES well, q_ν and q_δ are partition functions of the molecule's motions perpendicular and parallel to the surface, λ_{th} is the thermal wavelength of the free molecule [$\lambda_{th} = h/(2\pi mkT)^{1/2}$], and V_o is the binding energy of an isolated molecule on the surface. The lateral interaction between molecules on the surface, introduced in eq 5 as μ_i (here, for repulsion interactions $\mu_i > 0$), is described in our simulation with a lattice-gas model.[15] The surface is divided into an array of 2-D cells of area a_S , each containing one adsorption site. Due to the surface geometry and the location of the adsorption sites at steps, our lattice gas will have a rectangular geometry. The most important lateral interactions are shown in Figure 5: V_1 is the nearest-neighbor interaction energy along the step, V_{1p} is the nearest-neighbor interaction potential across the terrace, V_2 is the diagonal interaction across the terrace, and V_t is the trio interaction. We treated the lateral interaction within the "minimum cluster" approximation, which takes into account correlations among nearest neighbors, next-nearest neighbors, and triangular trio sites, following the approach of Hill[16] and Li.[17] For the rectangular geometry, the interaction chemical potential is

$$\mu_i = 2kT\ln\frac{z_1(1-\theta)}{\theta} \quad (6)$$

where z_1 is the solution of

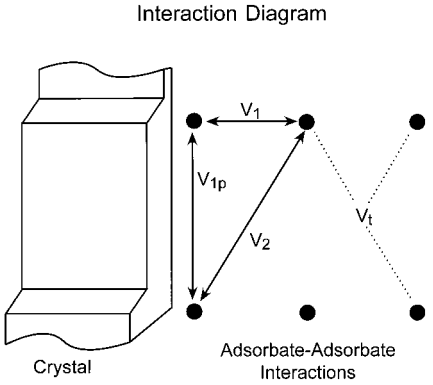

Figure 5. Lateral interaction diagram for a system of chemisorbed species localized at step sites on a periodic stepped surface. The filled circles represent the particles which interact laterally. The most important potentials characterizing the interaction are V_1 (nearest neighbor along the step), V_{1p} (nearest neighbor across the terrace), V_2 (next-nearest neighbor across the terrace), and V_t (trio interaction).

$$A^2(1-\theta)y_4^{\,2}z_1^{\,4} + A(3-4\theta)z_1^{\,3} + B(1-2\theta)z_1^{\,2} + (1-4\theta)z_1 - \theta = 0$$

$$A = y_1y_2y_3^{\,2}y_4$$

$$B = y_1 + y_2 + y_3^{\,2} \quad (7)$$

$$y_1 = \exp[-V_1/kT], \quad y_2 = \exp[-V_{1p}/kT]$$

$$y_3 = \exp[-V_2/kT], \quad y_4 = \exp[-V_t/kT]$$

The parameters used to simulate TPD curves with the models and approximations presented above are shown in Table 1. The computations were done with dedicated software.[18] A better treatment of the lateral interaction contribution would be that

TABLE 1: Energy and Adsorption Parameters Used in the Kinetic Lattice-Gas Simulations To Generate the TPD Spectra of N_2 Desorption from the Pt(335) and Pt(779) Surfaces Shown in Figure 4[a]

parameter	Pt(335)	Pt(779)	source
(1) binding energy, V_o (eV)	−0.515	−0.515	fit
(2) N_2–Pt stretching mode (cm^{-1})	200	200	fit
(3) N_2–step Pt site deformation mode (cm^{-1}) (degeneracy 2)	35	35	estimate based on refs 31 and 32
(4) N_2 intramolecular parameters			
(a) charact T_{vib}(free oscillator) (K)	3395	3395	ref 33
(b) charact T_{rot}(free rotor) (K)	2.87	2.87	ref 33
(c) charact T_{vib}(hindered oscillator) (K)	3218	3218	ref 1
(d) charact T_{rot}(frustrated rotor) (K)	158	158	desorption temp at zero coverage
(e) symmetry factor (free rotor)	2	2	
(5) repulsive lateral interaction (rectangular configuration)			
(a) nearest neighbor on step, V_1 (meV)	19	25	fit
(b) nearest neighbor across the terrace, V_{1p} (meV)	3.8	1.25	fit
(c) next-nearest neighbor across the terrace, V_2 (meV)	2.85	1.25	fit
(d) step−step−terrace trio, V_t (meV)	0.95	0	fit
(6) adsorption parameters			
(a) unit cell area (Å^2)	66.2	98.6	σ_{sat}^{-1}
(b) sticking coefficient, $S \simeq S_o[C_o + C_1\theta + C_2\theta^2 + C_3\theta^3 + C_4\theta^4]$			
S_o	0.907	0.678	this study
C_o	1.00	1.00	
C_1	1.84	0.332	
C_2	−11.52	−3.086	
C_3	22.77	8.134	
C_4	−14.06	−6.392	
(7) heating rate (K/s)	3.21	3.21	

[a] The simulation is based on the quasi-equilibrium approximation.[14,15] The lateral interaction is calculated with the minimum cluster method.[16,17]

of the "transfer matrix" method, which includes correlations between all the particles.[19] However, the transfer matrix method did not improve notably the character of the agreement between the measured and theoretical TPD curves shown in Figure 4. The simulation shows that the presence and behavior of the low-temperature desorption state are due to the dominance of the lateral repulsions between N_2(a) molecules on the desorption kinetics. The magnitudes of the various repulsion potentials are shown in Table 1. The simulated TPD curves reproduce very well the experimental desorption traces at low initial coverages. At higher coverages, we note a serious departure between theory and experiment, which we attribute to a systematic experimental error. This error is due to adsorption on the backside of the crystal, which contains the alternate stepped surface. Adsorption on the back would be expected to occur to a much lower coverage than on the front and would increase the relative contribution of the high-temperature state compared to the low-temperature state, as is in fact observed in Figure 4.

Because of the systematic error due to adsorption on the back of the crystal, it is not possible to analyze the experimental curves completely. Therefore, a set of theoretically generated curves with the same peak temperatures and peak widths as found experimentally (but having different peak intensities) were analyzed to qualitatively capture the actual desorption kinetic parameters. The desorption activation energies and the Arrhenius prefactors as a function of coverage were determined from a family of 30 simulated TPD traces of different initial coverage using the isosteric analysis (or the "complete analysis").[20] The isosteric rates have distinct values because the isosteric desorption temperature is different every time the initial coverage is changed. All the isosteric desorption rate/temperature pairs taken from the 30 simulated TPD traces are used to prepare an Arrhenius plot derived from the Polanyi−Wigner form of the rate equation:

$$\ln \frac{r}{\theta^n} = \ln \nu(\theta) - \frac{E_d(\theta)}{RT} \qquad (8)$$

where r is the rate, θ is the fractional coverage, n is the desorption order, E_d is the desorption activation energy, and ν is the preexponential factor. The isosteric analysis for first-order kinetics was performed by the computer with dedicated software,[18] and the results are shown in Figure 6. We compared the analysis of the simulated desorption curves with an analysis of the experimental curves in the leading-edge region.[21,22] Given the errors we encounter in the TPD experiment, the leading-edge analysis works satisfactorily only for the lower-coverage

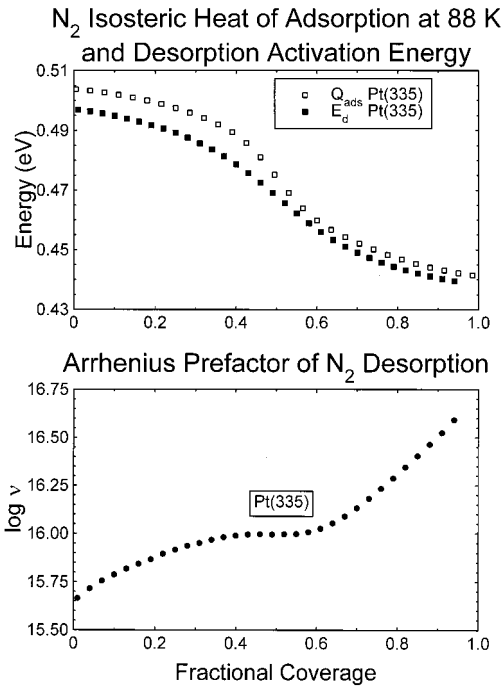

Figure 6. Activation energy of N_2 desorption and isosteric heat of N_2 adsorption (upper panel), and the Arrhenius prefactor (lower panel) for N_2 desorption from the Pt(335) surface. All points were determined from simulations within the kinetic lattice-gas model using the parameters displayed in Table 1. Simulations for the Pt(779) give values essentially identical with those for Pt(335) and are not shown.

TPD traces.[22] The desorption activation energy at zero coverage determined by the leading-edge analysis from the experimental curves is $E_d(\theta=0) = 0.49 \pm 0.06$ eV (error bar $\pm 2\sigma_{n-1}$) for both Pt surfaces under investigation, in excellent agreement with the isosteric analysis of the simulated curves ($E_d(\theta=0) = 0.50$ eV), as can be seen in Figure 6.

The isosteric heat of adsorption in Figure 6, Q_{iso}, was calculated from the same adsorption and energy parameters shown in Table 1 and the lattice-gas model described above.[16,17] The definition of the isosteric heat of adsorption and its connection to the chemical potential are given by

$$Q_{iso}(\theta,T) = kT^2\left(\frac{\partial \ln p}{\partial T}\right)_\theta = \frac{5}{2}kT + kT^2\left(\frac{\partial(\mu/kT)}{\partial T}\right)_\theta + kT^2\left(\frac{\partial \ln Z_{int}}{\partial T}\right)_\theta \quad (9)$$

where p is the pressure and $Z_{int} = Z_{vib}Z_{rot}$ is the rovib partition function of the gas phase.

The simulation yielded E_d, Q_{iso}, and $\log(\nu)$ curves for the Pt(779) surface essentially identical with those shown for Pt(335) in Figure 6. There was no sensible difference beween these thermodynamic and kinetic properties for the two Pt surfaces within the accuracy of our simulation.

IV. Discussion

A. Saturation Coverage. The N_2 adsorption measurements enabled us to determine the absolute coverage versus N_2 exposure and to postulate a mechanism for adsorption. First, we note that the ratio of the saturation coverage on the two Pt surfaces is $[\sigma_{335}^{sat}/\sigma_{779}^{sat}] = 1.49 \pm 0.25$, and this value is consistent with our previous report that N_2 adsorbs exclusively at step sites in the atop configuration.[1] If N_2 adsorbed only on terrace sites, the ratio should be close to 0.5, and if N_2 adsorbs on both types of sites, the ratio should be close to 1, assuming equal N_2 fractional coverage on the two surfaces. However, the ratio deviates significantly from the simplistic value of 2 given by the ratio of the number of step sites available on Pt(335) and Pt(779) surfaces. The fractional saturation coverage on the Pt(335) surface is 38% of the total number of step sites, while on the Pt(779) surface the fractional saturation of step sites is 52%. This difference shows that the local density of N_2 molecules on the steps is higher on the Pt(779) surface, perhaps due to a lower intermolecular repulsion energy across the terraces on the Pt(779) surface than on the Pt(335) surface, as indicated in Table 1.

B. Kinetics and Mechanism of Adsorption. The sticking probability is independent of coverage up to 70−80% of the saturation coverage, as shown in Figure 7 which was obtained from the data in Figure 3. This behavior is characteristic of adsorption through a mobile precursor—a physisorbed intermediate of low concentration and high mobility on the surface.[23] To understand the details of the mechanism of adsorption, various models are developed which can account for curve shapes such as the ones shown in Figure 7.

1. Phenomenological Kinetics. Phenomenologically, the global adsorption kinetics can be explained assuming the following: (1) the rate of adsorption is zero-order with respect to the empty chemisorption sites (always step sites[1]), and switches abruptly to first-order as the sticking probability starts to depend on the coverage; (2) there are terrace-bound adsorption precursors, because the initial sticking probability is higher than the fractional density of step sites on each surface; (3) there are also step-bound adsorption precursors, because the initial

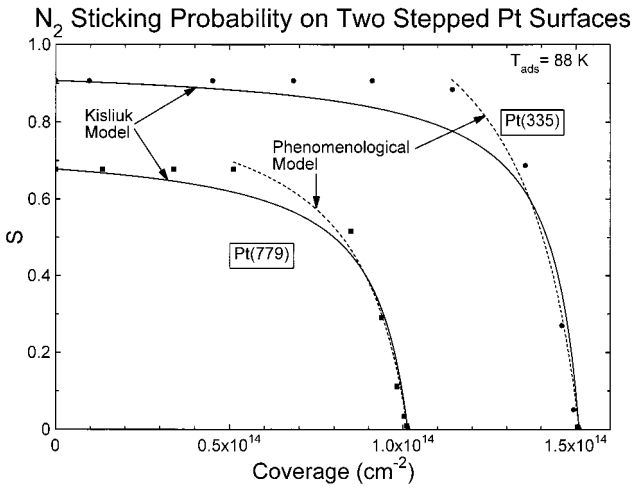

Figure 7. N_2 sticking probability on the two stepped surfaces, Pt(335) and Pt(779). The points represent derivatives of the uptake curves shown in Figure 3. The solid curves are Kisliuk fits (eq 12), with $K_{Pt(335)} = 0.054$ and $K_{Pt(779)} = 0.096$. The dashed curves represent fits of the coverage-dependent sticking probability to the phenomenological rate equation (eq 11).

sticking probability on the Pt(335) surface is higher than the fractional density of the terrace sites, and up to ~80% coverage the sticking probability is constant (the same assumption applies to the Pt(779) surface because the N_2 thermodynamics on Pt step sites are the same; see the Thermodynamics section). Assumption 3 is equivalent to saying that adsorption on step sites occurs through both extrinsic and intrinsic precursors present on the step sites. A situation with *only* intrinsic precursors at the step sites should give a strongly coverage-dependent sticking probability. Alternatively, Langmuirian adsorption kinetics on step sites with precursors *only* on terrace sites should also give a coverage-dependent sticking probability proportional to $1 - \theta$.

A recent report has shown that N_2 can easily be physisorbed on a Pt(111) surface below 60 K, giving an X-ray photoelectron spectral signature at 403.5 eV.[4] Experiments of this type are usually considered proof of isolation of intrinsic precursors.[23] Since intrinsic precursors exist on Pt(111) terrace sites, it is very likely that they also exist on Pt(100) step sites, perhaps in the troughs, where the N_2–Pt interactions are stronger.

The general kinetic model proposed for this system is shown in the following diagram: where G is the gas phase, T* is the

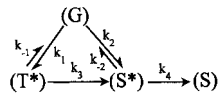

precursor on the terrace sites, S* is the precursor on the step sites, S is the chemisorbed phase on the step sites, and k_i are rate constants. The chemisorption step (k_4) cannot be set partially reversible as that situation would give the expression of an effective sticking coefficient, which depends on the coverage. In this model, the S* precursor never converts into the T* precursor, but either chemisorbs or desorbs. The sticking probability close to 1 observed for the Pt(335) surface supports this assumption. As a further simplification in this model, the step-bound extrinsic and intrinsic precursors are rendered indistinguishable in the formal treatment; therefore, the steady-state coverage of the step precursors will only depend on the density of step sites.

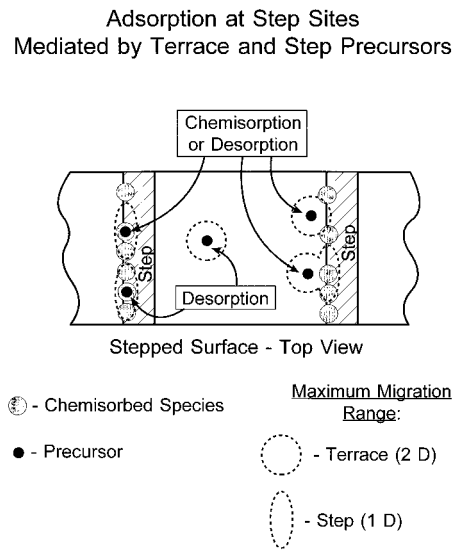

Figure 8. Picture of the step adsorption mechanism mediated by terrace and step precursors. Within their average lifetime, the precursors can sample only a maximum range of surface area shown by dashed circles, for 2-D sampling on terraces, and ovals, for 1-D sampling on steps. If they find an empty step site, the precursors may chemisorb with a certain probability; if they do not, they desorb. At low coverage, the kinetics have a nontrivial relation to the fraction of empty sites, $1 - \theta$, depending on factors such as the average lifetime of a given type of precursor and the lateral interaction forces between the precursor and the chemisorbed species and within the chemisorbed phase. At high coverage, the kinetics are proportional to the fraction of empty step sites ($1 - \theta$, pseudo-Langmuirian), because only the precursors which are close to an empty site may find it and chemisorb within their lifetime.

The rate equation for the last step is

$$\frac{d\sigma}{dt} = k_4 \sigma_{S^*}(\sigma_{sat} - \sigma)^n \qquad (10)$$

where σ is the absolute coverage of chemisorbed N_2 on the step sites (cm^{-2}), σ_{sat} is the N_2 saturation coverage, and n is the partial adsorption order, set to either 0 or 1, as has been discussed above. After using the steady-state approximation for T* and S*, the sticking probability becomes

$$S = \frac{d\sigma}{F\,dt} = \frac{k_2 + k_1 k_3 N_T/(k_{-1} + k_3 N_S)}{k_{-2} + k_4(\sigma_{sat} - \sigma)^n} k_4 N_S (\sigma_{sat} - \sigma)^n \qquad (11)$$

where F is the N_2 flux in the gas phase, N_T is the density of terrace Pt atoms, and N_S is the density of the step Pt atoms on the surface. In the early stages of adsorption, n is set to zero and the sticking probability predicted by eq 11 is indeed a constant, as observed in the first 70−80% of the adsorption process. For $n = 1$, the model gives a good description of the descending part of the sticking probability curve, shown in Figure 7 by dashed lines. The conversion from the $n = 0$ to the $n = 1$ rate law depends on the fact that the sticking probability starts to depend on coverage when the average size of the covered regions (the 1-D step N_2 domains) becomes sufficiently large such that the probability for the extrinsic precursor to find an empty chemisorption site within its lifetime drops considerably. This situation is pictured in Figure 8. According to eq 11, the magnitude of the initial sticking probability, $S_o(\sigma=0)$, depends on the relative density of step and terrace sites, N_S and N_T, but their action is not very obvious.

The phenomenological model was able to capture all the essential features of the mechanism of adsorption and the influence of the density of terrace and step sites. However, it could not predict the point of discontinuity between the two adsorption orders.

2. Statistical Kinetics: Connection to the Kisliuk Model. We attempt to explain the kinetics with a simple statistical model for random sequential occupation of sites, proposed by Kisliuk.[24] In the statistical approach, the sticking probability is defined as the sum of the probabilities of chemisorption of one molecule landing on a surface and being trapped as a precursor, on all the sites visited within the lifetime of the precursor. The intrinsic and the extrinsic precursors can easily convert into one another with no activation barrier. However, the two types of precursors are kinetically inequivalent, because only the intrinsic precursor can lead to chemisorption, and therefore the two precursors have different desorption and migration probabilities. The model assumes that the trapping probability of molecules from the gas phase into either intrinsic or extrinsic precursor states is unity, and that there are no lateral interactions between the chemisorbed species, either within the chemisorbed phase or within the precursor states. The kinetics derived from this model give the following sticking probability:

$$S = S_o\left(1 + \frac{\theta}{(1-\theta)}K\right)^{-1} \qquad (12)$$

where θ is the fractional coverage and $K = P_d'/(P_c + P_d)$; (P_c and P_d are probabilities of chemisorption and desorption, respectively, of the intrinsic precursor and P_d' is the desorption probability of the extrinsic precursor). The factor K is the Kisliuk constant, which depends on the adsorbate−substrate system.[24] The sticking probability always decreases monotonically with increasing coverage, giving a linear dependence for Langmuirian kinetics, or concave curvatures for $K > 1$ and convex curvatures for $K < 1$. Our data in Figure 7 resemble the $K < 1$ situation, for which Kisliuk's model requires the presence of both types of precursor states, extrinsic and intrinsic. The fits given by eq 12 are shown in Figure 7 by solid lines. The agreement between the fits and our experimental data is good only at very low or very high coverage, where the occupation of sites is quasi-random, as required by the model. The fits show significant deviation at intermediate coverages, which we attribute to lateral attractive interactions between the precursors and the chemisorbed admolecules. At intermediate coverages, the sticking probability is higher than that predicted by the Kisliuk model, indicating a higher probability of chemisorption for the intrinsic precursor as the chemisorbed phase builds up. The origin of the higher chemisorption probability may be the attractive force exerted on the intrinsic precursor, preventing it from departing from the chemisorbed island and forcing the precursor to spend a longer time on vacant sites near the chemisorbed admolecules. Because the site occupation is not random, as assumed by the model, the values of $K_{Pt(335)}$ and $K_{Pt(779)}$ differ from each other, which is an unreasonable expectation given that $K = P_d'/(P_c + P_d)$, and the N_2 thermodynamics on the two stepped Pt surfaces are the same (see the Thermodynamics section).

The statistical model must be corrected to explain differences in the initial sticking coefficients on the Pt(335) and Pt(779) surfaces. In the original model, $S_o = P_c/(P_c + P_d)$, where the P's on the right-hand side are probabilities of chemisorption and desorption, respectively, of the intrinsic precursor from any

site. The thermodynamics of N_2 adsorption on the two stepped surfaces, however, are the same, and the two initial sticking coefficients should be equal. To modify the kinetics, we incorporate in the model the fractions of sites and the transfer probability of a terrace precursor onto the step sites. With these corrections, the new kinetics are identical to eq 12, but now the parameters have different meanings: in the $K = P_d'/(P_c + P_d)$ constant, P_c is the chemisorption probability of an intrinsic precursor on an empty *step* site, P_d is the desorption probability of an intrinsic precursor from an empty *step* site, and P_d' is the probability of desorption of an extrinsic precursor from an occupied *step* site. The fraction of step sites affects exclusively the expression of S_o

$$S_o = \frac{X_S P_d^T + \beta(1 - P_d^T)}{P_d^T + \beta(1 - P_d^T)} \frac{P_c}{P_c + P_d} \tag{13}$$

which, in addition to the original Kisliuk $S_o = P_c/(P_c + P_d)$, contains another factor which depends on the fraction of the step sites, X_S, on the probability of the terrace precursor to migrate to a step site, β, and on the probability of desorption of the terrace-site precursor, P_d^T. Equation 13 predicts a lower initial sticking probability for surfaces with a smaller density of step sites, unless the desorption probability of the terrace precursor, P_d^T, is so small that it annihilates the contribution of X_S. A lower fraction of step sites also means larger average terrace width, which may decrease the probability of a terrace precursor to reach a step site, β, consistent with the intuitive idea of the competition between the average mobility range of a terrace precursor and the terrace width depicted in Figure 8.

In correcting Kisliuk's model for the inhomogeneous distribution of adsorption sites, we again assumed an irreversible conversion of the terrace precursor into the step precursor. This assumption is justified by other observations. Adsorption experiments of small molecules (such as CO and O_2) on stepped metal surfaces at low coverage, on surfaces where chemisorption is possible on both step and terrace sites (i.e., Pt), show that the chemisorbed phase is not statistically distributed between the two types of sites, but is always localized at steps.[25,26] Although the binding energy for chemisorbed species at step sites is larger than at the terrace sites,[27] the precursor states are not thermally equilibrated with the surface, and the occupation of sites should be more nearly statistical for the precursor species. We attribute the N_2 preferential occupation of step sites (as observed experimentally for CO and O_2) to the mobile N_2 precursors, which spend considerably more time at step sites than at terrace sites. Instead of having a random motion, the terrace mobile precursor experiences an attractive force toward the step troughs, where the interaction with the surface should be stronger. Once trapped at step sites, the mobile precursors move essentially in a 1-D space.

It has been pointed out[23,28] that a statistical treatment of the kinetics with averaged parameters that connect to phenomenological observables does not give more insight into the mechanism and should yield an equation equivalent to that derived for the phenomenological kinetics (i.e., from the rate law). Indeed, the statistical kinetic model presented above generated the same conclusions as the phenomenological model. In the statistical model, however, (1) the presence of extrinsic and intrinsic precursors follows naturally from the sticking probability curves, (2) there is no abrupt transition between two adsorption orders but just one smooth change with the coverage, and (3) the connection between the initial sticking probability and the fraction of step sites is easily understood.

There are better models for the sticking theory which include the lateral interactions between chemisorbed and trapped particles, and their correlation, for adsorption processes that are Markovian.[29] Such correlations are usually calculated within a kinetic lattice-gas model, by solving the equations of motion for the average occupation function.

C. Thermodynamics. The "pure" binding energy required to simulate properly the position of the higher-temperature desorption state of the experimental TPD curves is −0.515 eV (see Table 1). When the zero-point energies for the two Pt−N_2 soft modes (0.017 eV) are subtracted, the binding energy is essentially identical to the desorption activation energy at zero coverage, which is what eq 5 predicts when q_ν and q_δ are transferred into the exponential in the low-temperature approximation. The isosteric heat of desorption is just slightly larger than the desorption activation energy at zero coverage, and the two converge at saturation coverage within 0.004 eV (see Figure 6). This behavior can be understood by defining a differential E_d as

$$E_d = kT^2\left(\frac{\partial \ln R_d}{\partial T}\right)_\theta \tag{14}$$

and recalling that $R_d = S(\theta)a_S p/(2\pi mkT)^{1/2}$ in the quasi-equilibrium approximation. Comparing with eq 9, the connection of E_d to Q_{iso} is given by

$$E_d(\theta,T) = Q_{iso}(\theta,T) - \frac{1}{2}kT + kT^2\left(\frac{\partial \ln S(\theta,T)}{\partial T}\right)_\theta \tag{15}$$

Equation 15 allows us to calculate the temperature coefficient of the initial sticking probability: $(dS_o/dT)/S_o = -0.005\ K^{-1}$. Close to saturation coverage, the sticking probability becomes very small and its temperature dependence is essentially zero, bringing the difference between E_d and Q_{iso} down to $kT/2$, or 0.004 eV, at 88 K.

At saturation coverage on both stepped Pt surfaces, our simulation predicts a binding energy of −0.44 eV. For all practical purposes, the N_2 equilibrium thermodynamics on both surfaces are the same, irrespective of the terrace width. In a previous report, simulations of N_2 adsorption on a Pt(112) surface—which has narrower terraces than the Pt(335) surface and step sites identical with those of the same surface—by density functional theory gave a binding energy of −0.34 eV at 50% occupation of the step sites.[1] Part of this difference is due to the larger step−N_2 repulsive energies across the shorter terraces of Pt(112).

The Arrhenius prefactor curve in Figure 6 displays a sigmoidal shape, with an inflection point at $\theta = 0.5$. According to eq 5, the coverage dependence of the prefactor is controlled by the first two factors on the right-hand side, the sticking probability and the configuration term, $\theta/(1 - \theta)$. It is the $\log[\theta/(1 - \theta)]$ function that gives the sigmoidal shape and the inflection point at $\theta = 0.5$, showing that the overall increase of the Arrhenius prefactor is controlled by the configuration factor and is, therefore, an entropy effect. Indeed, the differential entropy change of N_2 adsorption, calculated from the isosteric heat of adsorption in Figure 6, decreases with coverage and displays the same inflection point (data not shown). More generally, eq 5 predicts that on a surface, within the quasi-equilibrium approximation, the Arrhenius prefactor always increases with increasing coverage as long as the sticking probability is a monotonically decreasing function of coverage.

Since the repulsive interaction between the N_2 strings localized at steps is small, our systems could be described

accurately by 1-D kinetic lattice-gas models built from Markovian processes which, for one-dimensionality, have essentially exact solutions.[30] Such a model was able to predict all the major characteristics we reported here for N_2 on stepped Pt surfaces: the shape of the TPD traces, the isosteric heat, and the Arrhenius prefactor curves.[30] Although our simulation was a 2-D approximation, it converged to the 1-D behavior by setting a large unit cell for the lattice gas (a_S) and small repulsion potentials across the terrace.

V. Conclusions

We have shown the following.

(1) N_2 chemisorbs on stepped Pt(335) and Pt(779) surfaces at 88 K with exclusive occupancy of step sites.

(2) The saturation coverage on the steps of the Pt(335) surface is 0.38 N_2/Pt atom; on Pt(779), the saturation coverage is 0.52 N_2/Pt atom. The increasing saturation coverage for increasing terrace width is caused by decreasing repulsive forces between step-bound N_2 molecules chemisorbed on adjacent steps as they become more widely separated across the terraces.

(3) The binding energy for a N_2 molecule on a step site is -0.50 eV at zero coverage, and decreases monotonically to -0.44 eV as the coverage on the steps increases. This is a consequence of lateral repulsive interactions between chemisorbed N_2 molecules, mainly along the steps.

(4) The initial N_2 sticking probability onto the stepped Pt crystals decreases monotonically as the terrace width increases. This is due to the finite range of terrace-bound N_2 precursors, which can desorb before reaching a step site.

(5) An irreversible conversion from 2-D precursor motion to 1-D precursor motion occurs as terrace-bound precursors irreversibly convert to step-bound precursors.

(6) These experiments suggest that the adsorption of N_2 on high-area Pt catalysts will be strongly influenced by stronger binding of N_2 at step sites and by adsorption kinetic effects which are enhanced as the defect density increases. The average precursor migration range from a smooth site region to a defective site region will control the efficiency of N_2 chemisorption at the defect sites.

Acknowledgment. We thank the Department of Energy, Office of Basic Energy Sciences, for supporting this work.

References and Notes

(1) Tripa, C. E.; et al. *J. Chem. Phys.* **1999**, *111*, 8651.

(2) Arumainayagam, C. R.; Tripa, C. E.; Xu, J.; Yates, J. T., Jr. *Surf. Sci.* **1996**, *360*, 121.

(3) Tripa, C. E.; Yates, J. T., Jr. *Rev. Roum. Chim.* **1999**, *44*, 1035.

(4) Zehr, R.; et al. *J. Phys. Chem. B* **2000**, *104*, 3094.

(5) Egerton, T. A.; Sheppard, N. *J. Chem. Soc., Faraday Trans. 1* **1974**, *70*, 1357.

(6) Shigeishi, R. A.; King, D. A. *Surf. Sci.* **1977**, *62*, 379.

(7) Zubkov, T. S.; Tripa, C. E.; Yates, J. T., Jr. *J. Phys. Chem. B* **2001**, *105*, 3733.

(8) Muha, R. J.; Gates, S. M.; Yates, J. T., Jr.; Basu, P. *Rev. Sci. Instrum.* **1985**, *56*, 613.

(9) Yates, J. T., Jr. *Experimental Innovations in Surface Science*; AIP Press, Springer-Verlag: New York, 1998; pp 604−613.

(10) Winkler, A.; Yates, J. T., Jr. *J. Vac. Sci. Technol., A* **1988**, *6*, 2929.

(11) King, D. A.; Wells, M. G. *Surf. Sci.* **1972**, *29*, 454.

(12) Madey, T. E. *Surf. Sci.* **1972**, *33*, 355.

(13) Smentkowski, V. S.; Yates, J. T., Jr. *J. Vac. Sci. Technol., A* **1989**, *7*, 3325.

(14) Payne, S. H.; Kreuzer, H. J. *Surf. Sci.* **1988**, *205*, 153.

(15) Kreuzer, H. J.; Payne, S. H. In *Dynamics of Gas−Surface Interactions*; Rettner, C. T., Ashfold, M. N. R., Eds.; Advances in Gas-Phase Photochemistry and Kinetics Series; The Royal Society of Chemistry: Cambridge, 1991; pp 220−256.

(16) Hill, T. L. *J. Chem. Phys.* **1950**, *18*, 988.

(17) Li, Y. Y. *Phys. Rev.* **1949**, *76*, 972.

(18) Astek 2.0: H. J. Kreuzer, S. H. Payne, Helix Science Applications, 1995.

(19) Payne, S. H.; Zhang, J.; Kreuzer, H. J. *Surf. Sci.* **1992**, *264*, 185.

(20) Falconer, J. L.; Madix, R. J. *J. Catal.* **1977**, *48*, 262.

(21) Habenschaden, E.; Küppers, J. *Surf. Sci.* **1984**, *138*, L147.

(22) Miller, J. B.; et al. *J. Chem. Phys.* **1987**, *87*, 6725.

(23) Weinberg, W. H. In *Kinetics of Interface Reactions*; Grunze, M., Kreuzer, H. J., Eds.; Springer Series in Surface Sciences, Vol. 8; Springer-Verlag: Berlin, Heidelberg, New York, London, Paris, Tokyo, 1987; pp 94−124.

(24) Kisliuk, P. *J. Phys. Chem. Solids* **1957**, *3*, 95.

(25) Hayden, B. E.; Kretzschmar, K.; Bradshaw, A. M.; Greenler, R. G. *Surf. Sci.* **1985**, *149*, 394.

(26) Stipe, B. C.; Rezaei, M. A.; Ho, W. *J. Chem. Phys.* **1997**, *107*, 6443.

(27) Hammer, B.; Nielsen, O. H.; Nørskov, J. K. *Catal. Lett.* **1997**, *46*, 31.

(28) Cassuto, A.; King, D. A. *Surf. Sci.* **1981**, *102*, 388.

(29) Kreuzer, H. J. *J. Chem. Phys.* **1996**, *104*, 9593.

(30) Payne, S. H.; Wierzbicki, A.; Kreuzer, H. J. *Surf. Sci.* **1993**, *291*, 242.

(31) Ahner, J.; Mocuta, D.; Ramsier, R. D.; Yates, J. T., Jr. *Phys. Rev. Lett.* **1997**, *79*, 1889.

(32) Braun, J.; et al. *J. Chem. Phys.* **1998**, *108*, 5161.

(33) Niac, G.; Voiculescu, V.; Bâldea, I.; Preda, M. *Formule Tabele Probleme de Chimie Fizică*; Editura Dacia: Cluj-Napoca, Romania, 1984; pp 109, 111.